Journal of
Materials Chemistry C

Accepted Manuscript

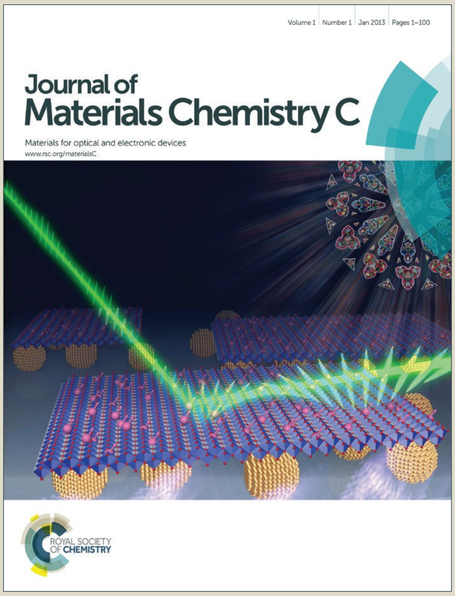

ROYAL SOCIETY
OF **CHEMISTRY**

www.rsc.org/materialsC

Organic-Inorganic Hybrid Semiconductor Thin Films Deposited using Molecular-Atomic Layer Deposition (MALD)

Jie Huang[a], Hengji Zhang[a], Antonio Lucero[a], Lanxia Cheng[a], Santosh KC[a], Jian Wang[a], Julia Hsu[a], Kyeongjae Cho[a], and Jiyoung Kim[a *]

[a] Department of Material Science and Engineering, the University of Texas at Dallas, Richardson, Texas 75080, USA.

ABSTRACT

Molecular-atomic layer deposition (MALD) is employed to fabricate hydroquinone (HQ)/diethyl zinc (DEZ) organic-inorganic hybrid semiconductor thin films with accurate thickness control, sharp interfaces, and low deposition temperature. Self-limiting growth is observed for both HQ and DEZ precursors. The growth rate keeps constant of approximately 2.8 Å/cycle at 150 °C. The hybrid material exhibits n-type semiconducting behavior with a field effect mobility of approximately 5.7 $cm^2/V{\cdot}s$ and an on/off ratio of over 10^3 following post annealing at 200 °C in nitrogen. The resulting films are characterized using ellipsometry, Fourier transform infrared spectroscopy (FTIR), transmission electron microscopy (TEM), UV-Vis spectroscopy, transistor behavior, and Hall-effect measurement. Density functional theory (DFT), and many-body perturbation theory within the GW approximation are also performed to assist explanation and understanding of the experimental results. This research offers a valuable candidate of n-channel materials for efficient organic CMOS devices.

KEYWORDS: Molecular-atomic layer deposition, organic inorganic hybrid film, semiconductor

1. Introduction

Organic-inorganic hybrid films have emerged as promising alternatives for next-generation electrical materials because of a number of their advantageous properties owing to the innovative combination of both organic and inorganic components. For example, organic materials offer advantages such as good flexibility, low-temperature processing feasibility, low-cost, and light-weight.[1] Whereas inorganic component serves as a linker facilitating formation of an extended framework bound by strong covalent or ironic interactions to provide high carrier mobility.[2] Previous researches have demonstrated fabrication of various organic-inorganic hybrid materials ranging from metal-organic-framework (MOF) to perovskite and nanowire based, i.e. 0-D and 1-D, hybrid materials.[3-5] However, studies of the electrical properties of these materials are desired prior to realizing potential applications in energy storage, gas adsorption, solar cells, and optoelectronic nano-devices.

Recently, molecular layer deposition (MLD) has been developed rapidly inspired by its great prospect in fabricating uniform and high quality hybrid organic-inorganic polymerized films.[6-8] The surface chemistry of MLD is based on sequential and self-limiting gas-phase surface reactions as proposed for atomic layer deposition (ALD), accordingly, allowing for a so-called conformal growth-per-cycle (GPC) behavior, ca. 1 Å/cycle, with molecular/atomic scale control over film thickness.[9-14] Due to its great flexibility in the selection of particular organic precursor of interest, MLD is feasible to deposit a variety of organic films with unique properties.[15-18] Particularly, B. Yoon et al. demonstrated that by applying inorganic metal precursors as those commonly used in ALD as linkers, it is feasible to fabricate hybrid organic-inorganic thin films in a process we refer as molecular-atomic layer deposition (MALD).[19] Moreover, unlike ALD or MLD, which exclusively featured with deposition of pure inorganic or organic films, MALD has extended from initial organic film specific technique to fabricate a wide range of hybrid organic-inorganic films consisting either laminated metal interlinked organic layers with identical length or alternating two-dimensional planes of inorganic and organic monolayers.[20-23] Among these polymerized hybrid materials reported so far, most of them have been focusing on the fundamental understanding of the surface chemistry between the bi-functional organic precursors including ethylene glycol, glycidol and alkylsilanes etc. with inorganic metal precursors like trimethyl aluminum (TMA), diethylzinc (DEZ) and titanium tetrachloride ($TiCl_4$), etc. in terms of growth rate, temperature, thermal stabilities, etc. However, there requires investigations on the electrical properties of these films to enlighten understanding their practical applications.

Herein we demonstrate the deposition of hydroquinone (HQ)/diethyl zinc (DEZ) organic-inorganic hybrid thin films using MALD. The multilayers were successfully formed at low temperatures with accurate control of film thickness and sharp interfaces. Our electrical measurements suggest that the resulting hybrid material demonstrated an n-type semiconductor behavior.

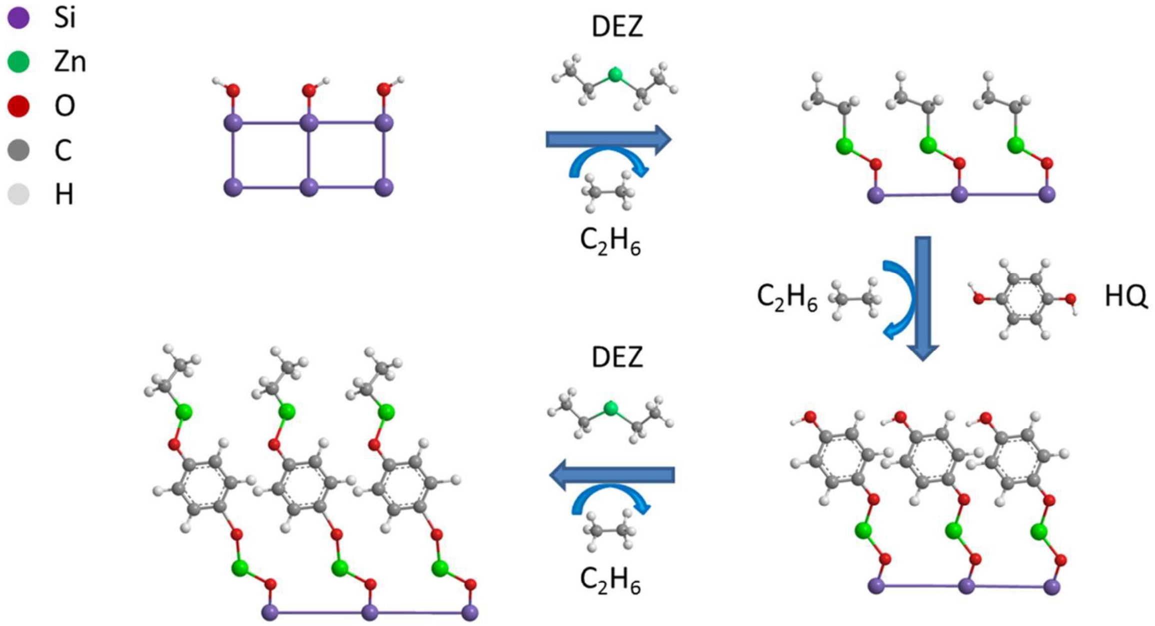

Figure 1. Schematic mechanism of HQ/DEZ hybrid thin film deposited by MALD.

The reaction mechanism for the HQ/DEZ hybrid thin film deposition is schematically illustrated in Figure 1. HQ molecules were deposited based on an exchange reaction between its –OH groups and the $–C_2H_5$ groups of DEZ. The self-limiting nature of the surface reactions between HQ and DEZ was examined by depositing 100 MALD cycles as a function of DEZ and HQ dosing time. Figures 2 (a) and (b) suggested that the HQ reaction on $–Zn–C_2H_5$ was self-limiting and reached saturation after 30 sec of HQ dosage; and DEZ reaction on –OH saturated after 1 sec of DEZ exposure, respectively. The long pulse time required for HQ pulse indicating the relatively low vapor pressure and/or low chemical reactivity of organic molecules. Whereas the short DEZ pulse time is comparable with typical ZnO deposition using DEZ and H2O, indicating the fast chemical reaction between ethyl group and –OH terminated surface.[24] Due to the incorporation of organic components, the refractive index of the resulting films was relatively low (approx. 1.7), compared to the value for ALD ZnO (approx. 2.0). The temperature dependence of the thin film growth is plotted in Figure 2 (c). The relative ALD temperature window is between 100 to 200 °C. Below 100 °C, there is insufficient thermal activation energy for chemical reaction to occur, while above 200 °C, thermal motion and disorder prevent the adsorbed organic molecules from self-assembling into ordered structures with the molecular backbone oriented normal to the substrate.[25-27] The growth rate, i.e. cycle dependent of film thickness, is plotted in Figure 2 (d). The growth rate is evaluated to be approx. 3 Å/cycle at 150 °C, which is slightly higher than similar deposition process reported elsewhere.[28] This obtained growth rate is fairly reasonable taking consideration of nucleation and geometric effects.[29-31]

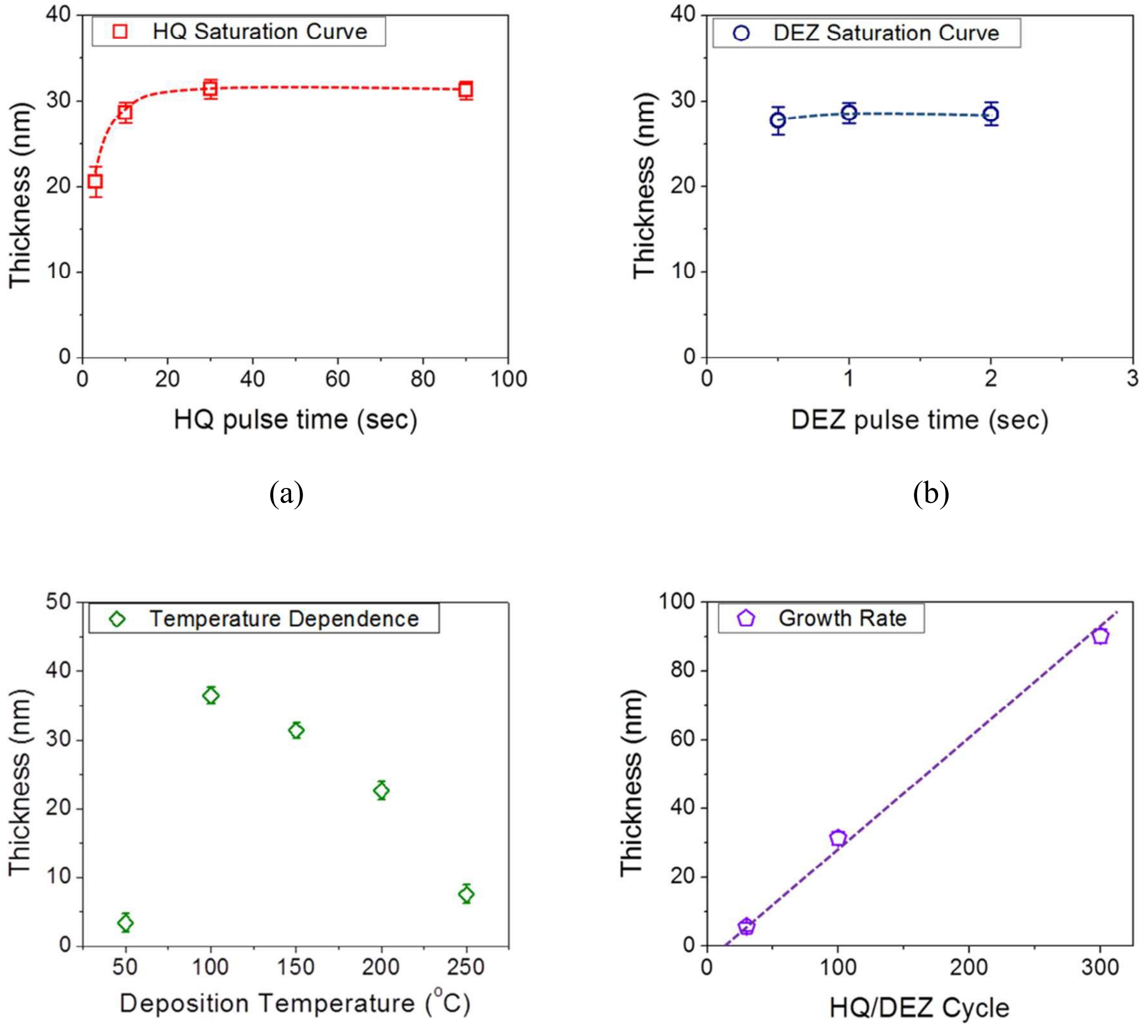

(a) (b)

(c) (d)

Figure 2. (a) HQ pulse saturation curve, (b) DEZ pulse saturation curve, (c) temperature dependence, and (d) growth rate confirmation of HQ/DEZ hybrid thin film deposited at 150 °C.

To confirm the chemical reaction between the HQ and DEZ precursors during MALD, FTIR spectroscopy was used to characterize the structural information of HQ/DEZ films deposited at 150 °C for 30, 100, and 300 cycles. As shown in Figure 3, two characteristic vibrational modes belonging to HQ molecular component are identified. And the peak intensities increased continuously upon increasing the numbers of MALD cycles. The higher frequency vibrational mode found at approx. 1500 cm^{-1} is assigned to the C=C stretches present in the aromatic ring of the HQ molecule,[32] and the lower frequency mode identified at approx. 1200 cm^{-1} corresponds to the C–O stretching vibration present in HQ after reaction with DEZ. The observation of these modes and the increase of their peak intensities provide direct evidence of the existence of HQ in the hybrid films. The O–H stretching mode, which is mainly arising from crystalline HQ molecule and is expected to give rise to a strong peak at approx. 3250 cm^{-1}, is examined in order to ensure the exchange reaction between –OH and –Zn–C_2H_5. As seen from the infrared spectra, there is no –OH mode detected from the obtained HQ/DEZ films, indicating the complete reaction of HQ with the DEZ, otherwise, –OH vibration from unreacted HQ molecule is likely to present. The C–H vibration in aromatic ring is at 823 cm^{-1}, which is right below our conventional FTIR detection limit (approx. 1000 cm^{-1}). Also notice that there is a tiny peak located around 3050 cm^{-1}, which agrees with the intrinsically weak C–H stretch mode in the aromatic compound (3000~3100 cm^{-1}). Direct observation of the hybrid thin film was confirmed by cross-sectional TEM of the HQ/DEZ deposited for 100 cycles. As clearly demonstrated in Figure 4, 100 cycles of HQ/DEZ lead to the formation of very uniform layer of organic-inorganic hybrid films. Since the MALD is carried out at 150 °C, the film has an amorphous nature. Based on the image contrast, the thickness of the HQ/DEZ layer is measured to be 28 nm, equivalent to the estimated value based on ellipsometry data (approx. 30 nm).

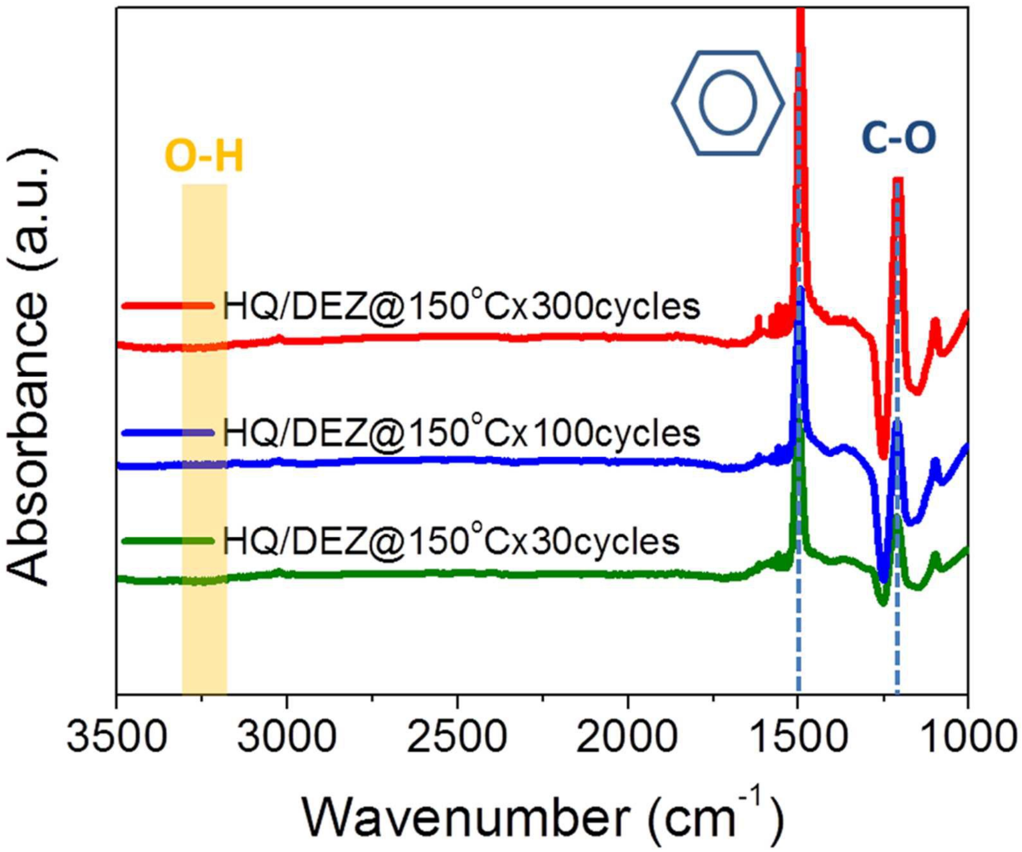

Figure 3. FTIR spectra of HQ/DEZ hybrid thin films deposited for 30, 100, and 300 cycles at 150 °C.

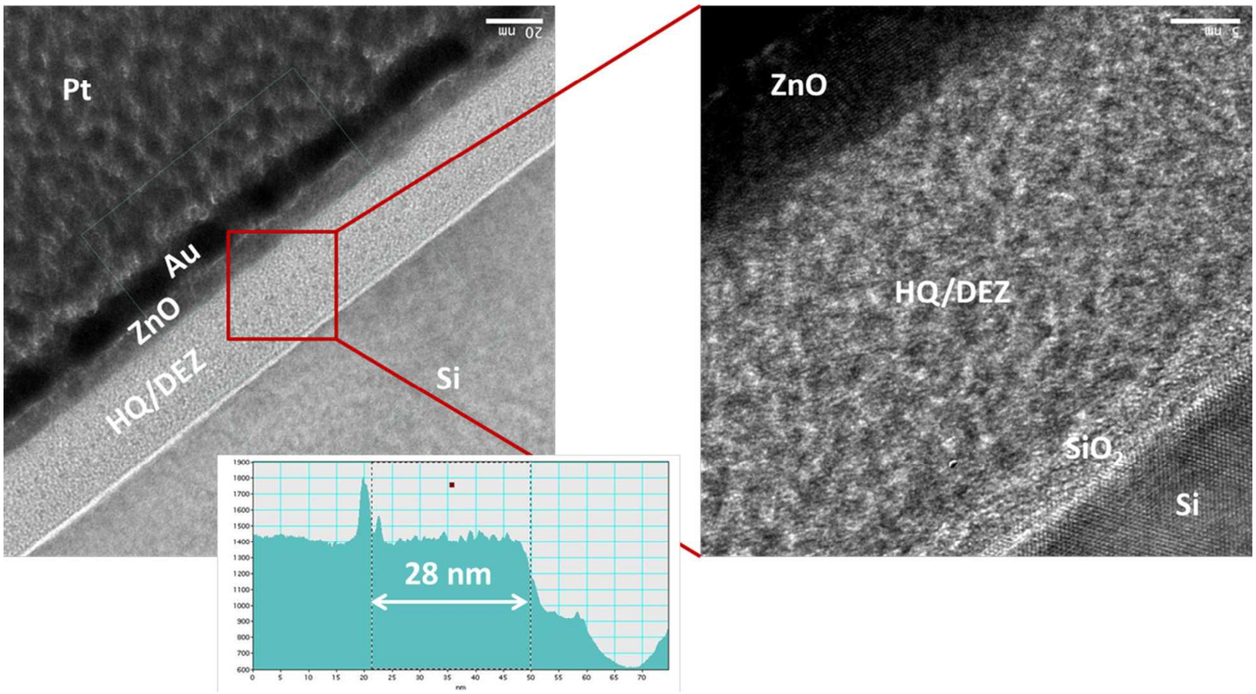

Figure 4. Cross-sectional TEM image of HQ/DEZ hybrid thin film deposited at 150 °C for 100 cycles. Inset is the contrast profile of HQ/DEZ between silicon substrate and ZnO cap layer.

As mentioned earlier, organic-inorganic film could exhibit distinctive properties in contrast to its inorganic counterparts due to the inclusion of organic components. Herein, UV-Vis measurements were performed on the HQ/DEZ hybrid thin films deposited on glass substrates (PEARL) at 150 °C for 300 cycles. Reference spectrum was prepared using pure ALD-ZnO films deposited at the same temperature for the same number of cycles using DEZ and water as precursors. As shown in Figure 5, both samples are transparent in the visible region from 400 to 900 nm, with one or more absorption edges in the UV region between 300 to 400 nm. The optical bandgap is estimated using the Urbach model[33] by fitting the absorption coefficient α to Eq. (1):

$$\alpha = A * (h\nu - E_g)^{1/2} \dots \dots (1)$$

where A is a constant related to the refractive index and the electron/hole effective masses, h is Planck's constant, v is wave frequency, such that hv is the photon energy, and E_g is the bandgap of the material.[34] The energy band gap between the valence band maximum (VBM) and the conduction band minimum (CBM) for the HQ/DEZ hybrid thin films is estimated to be approx. 3.16 eV from the adsorption edge. In contrast, the calculated band gap of ALD-ZnO film deposited at the same temperature is approx. 3.21 eV. Another less distinctive absorption band is observed below 350 nm in the HQ/DEZ films, but not in ZnO. This higher energy band may be attributed to π-π transition band.[35]

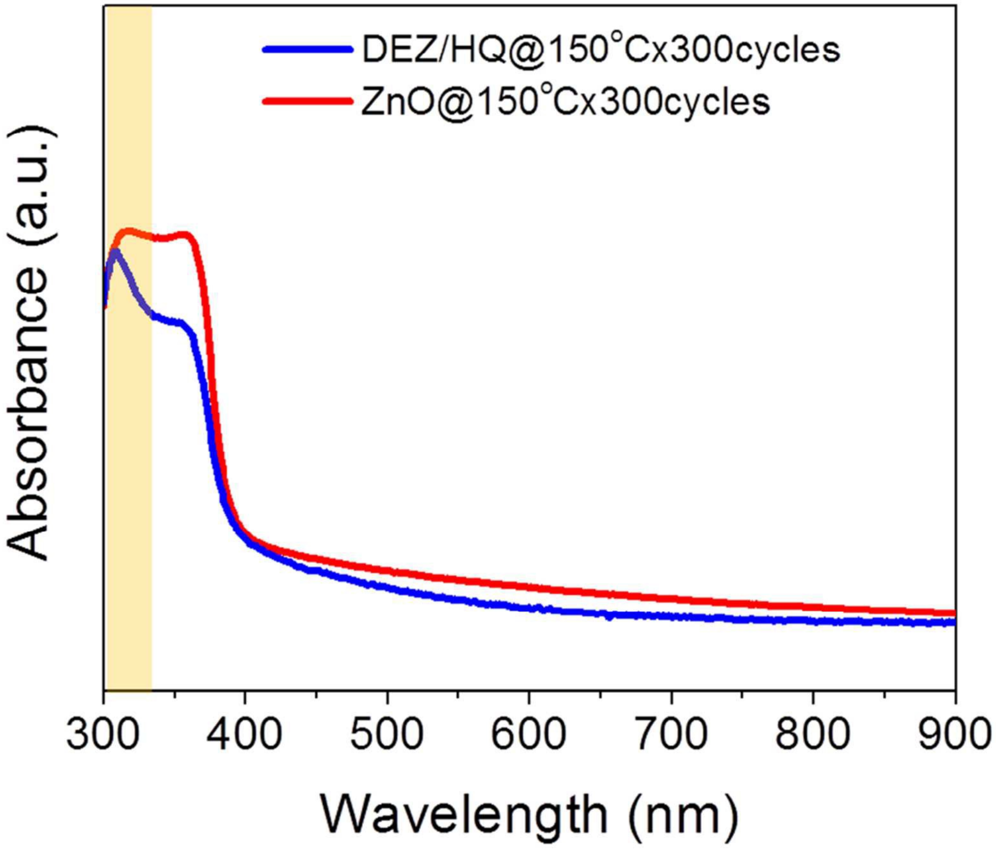

Figure 5. UV-Vis spectra of HQ/DEZ hybrid and pure ZnO thin films deposited at 150 °C.

According to UV-Vis absorption spectra, the photo excitation behavior of HQ/DEZ hybrid film is different from that of ZnO inorganic film. This indicates that our synthesized organic-inorganic hybrid thin film may have unique optical and/or electrical properties. It remains challenging to provide direct experimental evidence confirming the structural ordering of HQ and DEZ molecules in the hybrid system, even though the good agreement between experimental film growth rate and that from estimation seems to suggest a very likelihood of densely packed structures. To overcome this experimental challenge, we have performed first-principles calculations to investigate the electrical and optical properties of HQ/DEZ and other potential by-product molecules.

Using G^0W^0 approach, we calculated the quasiparticle band structures for 1-D molecules, HQ/DEZ, as shown in Figure 6 (a). It demonstrates that HQ/DEZ has a direct band gap of 3.86 eV. We have also determined HUMO-LUMO gap for single HQ molecule as 8.89 eV. Based on these distinguishable electronic structures, HQ seems not to be the by-product, because its band gap is apparently much larger than that of other materials. When comparing our calculation with experimental results, we find that our calculated band gap (3.86 eV) for HQ/DEZ is close to the larger band gap (3.71 eV) measured for as-deposited HQ/DEZ. Meanwhile, the smaller band gap (3.16 eV) for as-deposited HQ/DEZ is similar to the band gap of ZnO, i.e. according to previous GW calculation, the band gap of ZnO is approx. 3.2 eV,[36] which is close to our experimental results. At room temperature, phase separation is unlikely to happen for HQ/DEZ. Therefore, we believe that HQ/DEZ itself can demonstrate two peak intensities without contribution from crystalline ZnO. In order to examine this hypothesis, we have calculated photo optical spectrum of 1-D HQ/DEZ molecule based on G^0W^0-BSE method. It reveals that multiple photo excitation gaps are possible for HQ/DEZ, as shown in Figure 6 (b). The energy difference between the first peak (E_1=3.9 eV) and second peak (E_2=4.85 eV) is approx. 0.9 eV. Our simulation on photo excitation spectra suggests that the two peak intensities observed in experiment are possible for HQ/DEZ.

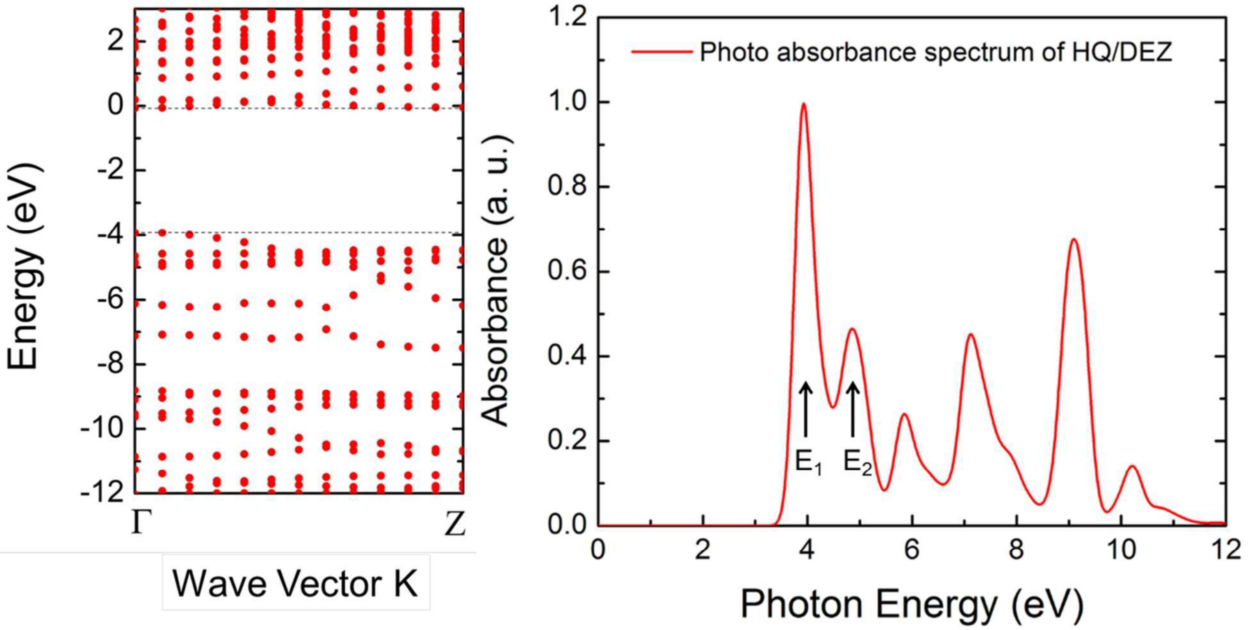

(a) (b)

Figure 6. (a) The quasiparticle band energy structures for one dimensional HQ/DEZ, and (b) the photo absorbance spectrum of HQ/DEZ.

Even though organic-inorganic hybrid films have been demonstrated in other MLD/MALD studies, few have explored the corresponding electrical behavior which is important for nano-electronic application. Before investigating transistor behavior of HQ/DEZ films, the transmission line method (TLM)[37] was applied to ensure an Ohmic contact between metal and semiconductor (see S.1). It also has been widely demonstrated that annealing improves the metal-semiconductor contact (from Schottky to Ohmic), as well as the crystallinity and molecular ordering of organic/hybrid thin films.[38] We have confirmed the HQ/DEZ hybrid thin film is thermally stable up to 200 °C (see S.2). The field-effect charge transport properties of the HQ/DEZ films were investigated by fabricating and testing TFTs with bottom gate and top contact architecture, as shown in Figure 7 (a) and (b). The TFT channels are 300 μm in width and 50 μm in length. The HQ/DEZ TFTs post-annealed at 200 °C exhibited typical n-type behavior with good current modulation in the output and transfer characteristics, as shown in Figure 7 (c) and (d), respectively. The I_D-V_D curve in Figure 7 (c) indicates that at V_G=30 V and V_D=40 V, I_D reaches to approximately 400 μA. The I_D-V_G curve in Figure 7 (d) demonstrates an I_{on}/I_{off} ratio of over 10^3 could be obtained for the HQ/DEZ TFTs. The electron mobility was calculated from the transfer characteristics by fitting a straight line to the I_D-V_G curve according to Eq. (2), which is valid in the linear region:

$$\mu_{lin} = m_{lin}\frac{L}{W}\frac{1}{V_{DS}}\frac{1}{C_i} \dots\dots (2)$$

where m_{lin} is the slope of the straight fitting line, L and W are the channel length and width, and C_i is the capacitance per unit area of the gate insulator, i.e. silicon dioxide (SiO_2) in our case. For V_{DS}=1 V, the electron mobility μ_{lin} was 5.7 cm^2/V·s, which is approx. 10 times higher than classic spin-coated perovskite hybrid semiconductor.[2] The high mobility obtained from our hybrid MALD films has demonstrate rather good n-channel TFTs performance, which is comparable to that of high-performance organic p-channel devices, even though the contact resistance was somewhat large, in this case, which might be attribute to the presence of less favorable the energy levels line-up at the contact/semiconductor interfaces in contrast to the optimized p-channel TFTs.[39, 40]

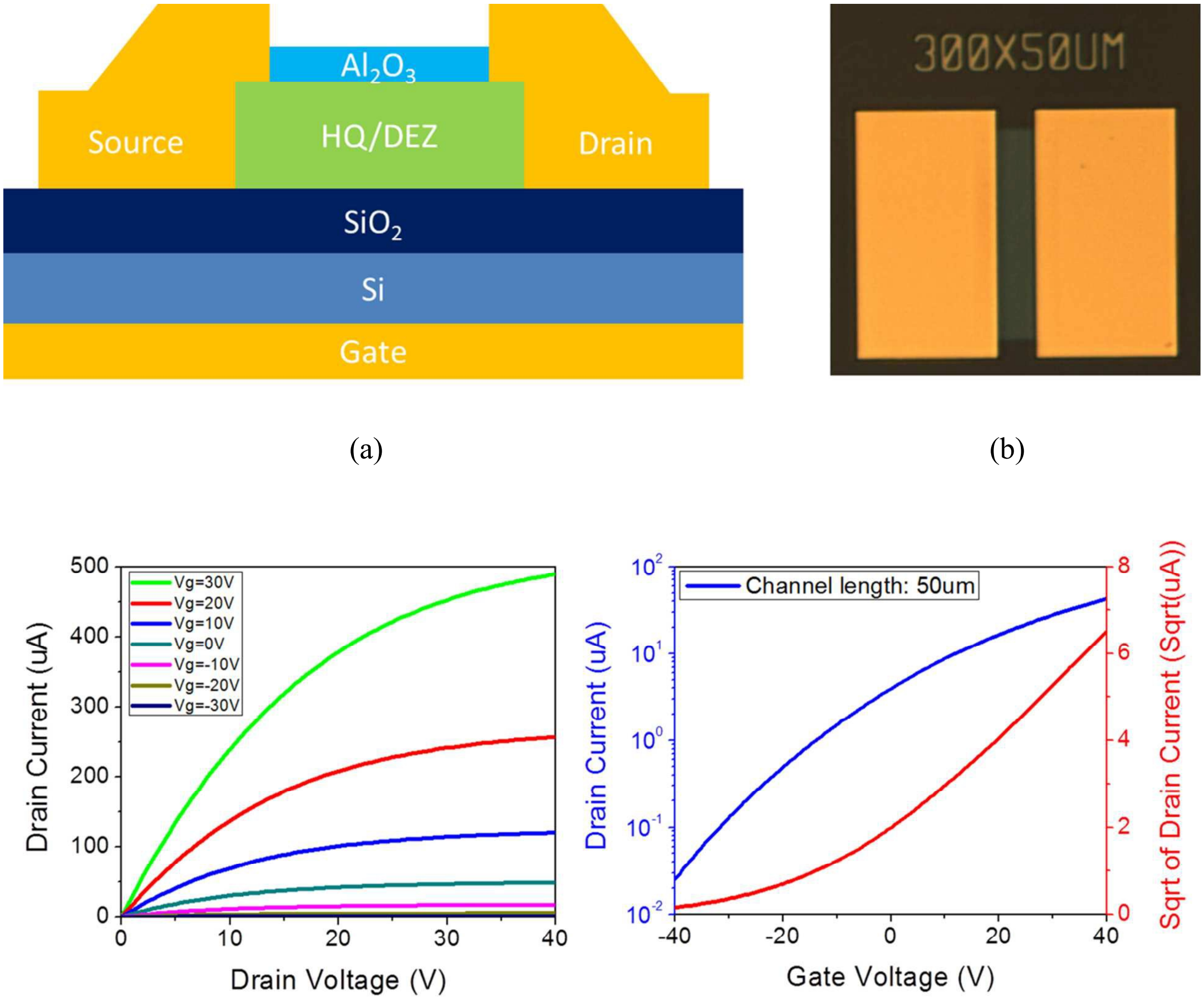

(a) (b)

(c) (d)

Figure 7. (a) Schematic side view and (b) actual top view of TFT device structure using HQ/DEZ hybrid thin film as channel layer, and TFT device performance (c) out-put curve and (d) transfer curve of HQ/DEZ hybrid thin film as channel layer at room temperature.

The conduction mechanism in these films remains a topic of discussion. To the best of our knowledge, we tend to believe that the charge transport is mostly likely arising from the presence of oxygen vacancies (V_o) in the hybrid films resembling to the mechanism proposed for ZnO films.[41, 42] In our HQ/DEZ films, the rising of the relative high electron mobility might be ascribed to the introduction of aromatic rings from the reaction between HQ and DEZ precursors. As the π-π stacking effect from the aromatic rings favors strong intermolecular interactions, which can result in considerably high degree of solid state ordering and molecular packing between HQ/DEZ chains that govern the charge carrier transport across the intra and intermolecular network of the hybrid thin films. With improved packing through reinforcing intramolecular interactions, enhanced molecular π-orbital overlap could be achieved.

Stabilizing the electrons during FET operation in the absence of device encapsulation is a major challenge in designing n-channel organic materials.[43] Degradation of such materials in the ambient atmosphere is suspected to be result from the reaction of the charge-carrying electrons with O_2 and H_2O, rather than the intrinsic chemical instability.[44] Therefore, an Al_2O_3 passivation layer was deposited to minimize air exposure of the hybrid active channel layer during storage and post annealing.

The temperature dependence of the field-effect properties of Al_2O_3 passivated HQ/DEZ films were also performed (see S.3). The mobility decreased obviously upon increasing measurement temperature, as shown in Figure 8. The inverse relationship between the electron mobility and temperature may be attributed to the lattice vibration induced carrier scattering at elevated temperatures. In addition, traps attributed to structural defects are another important factor impacting the transport of charge carriers in polycrystalline/amorphous films. Nevertheless, the effective electron mobility was still above 1 $cm^2/V\cdot s$ even at a temperature of 150 °C. Further optimization of HQ-DEZ films is required to achieve high on/off ratio and low off current for TFT applications.

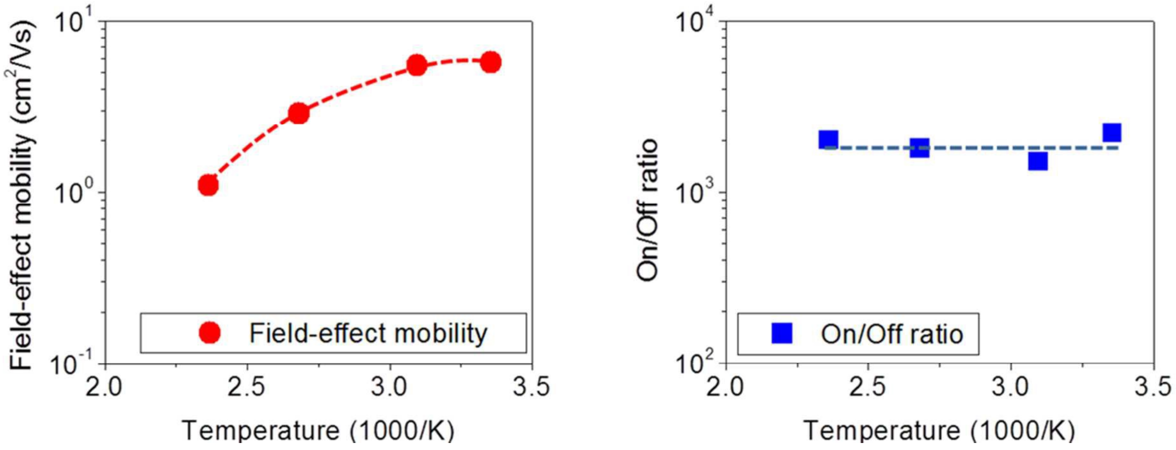

(a) (b)

Figure 8. Temperature dependence of (a) field-effect mobility and (b) on/off ratio of HQ/DEZ TFT.

Hall-effect measurement was performed to confirm the electron mobility using the HQ/DEZ thin film of the same thickness for TFT devices. All samples exhibited n-type characteristics. The Hall-mobility is approx. 1.73 $cm^2/V{\cdot}s$ at room temperature and a carrier concentration of approximately $4.6 \times 10^{18}/cm^3$ is extracted. These values obtained directly from Hall-effect measurement. μ_{Hall} is relatively lower than RT μ_{TFT}, which might be caused by the difference between device dimensions. Because OTFTs are interfacial devices whose performance is highly dependent on the interface between the organic semiconductors and the gate dielectrics,[45] and in n-type OTFTs almost all charge transport occurs in the first few layers located near the dielectric/organic layer interface.[46] In this work, the Hall-bar pattern was 20 times longer than the TFT channel. Thus, the scattering at the interface between the HQ/DEZ thin films and the substrate would become even more dominant and apparent, resulting in lower electron mobility.

In summary, we have fabricated high quality of HQ/DEZ organic-inorganic hybrid thin films using MALD and investigated the electrical properties of these materials. Our experimental findings demonstrated that hybrid thin films have been successfully deposited on Si substrate by using MALD of HQ and DEZ at low temperature of 150 °C, in which the HQ molecule are likely self-limiting, well-organized and densely packed as indicated by the comparable growth rate of 3 Å/cycle. Density functional theory (DFT), and many-body perturbation theory within the GW approximation were also performed to assist explanation and understanding of the experimental results, thus to confirm the existence of organic-inorganic hybrid material. Using this MALD approach, a novel hybrid n-type semiconducting material with field-effect electron mobility above 5 $cm^2/V{\cdot}s$ at room temperature was achieved. The resulting material is a potentially valuable candidate for producing efficient n-channel materials in organic complementary circuits.

Experimental Section

Silicon (100) wafers (Silicon Valley Microelectronics) were used as substrates. After removing the native oxide using 1 % HF, approximately 90 nm of thermal oxide was grown on the substrate for TFT devices and approximately 300 nm of thermal oxide was grown for Hall-effect measurements. Prior to deposition, the substrates were treated using UV light combined with ozone (O_3) gas for 5 min to remove potential organic contaminants and achieve better hydrophilic surface.

The organic-inorganic hybrid films were deposited using a D100 (NCD Tech, Daejeon, Korea) at 150 °C, unless mentioned otherwise. The flow rate of the N_2 carrier gas was 50 sccm. Hydroquinone (HQ, Sigma-Aldrich, 96%) powder was placed in a stainless steel canister and evaporated at 130 °C. The DEZ (Sigma-Aldrich) precursor was evaporated at 20 °C. The MALD cycle consisted of 1 sec exposure to DEZ, 20 sec of N_2 purge, 30 sec exposure to HQ, and 60 sec of N_2 purge.

Spectroscopic ellipsometry (Sentech 800) was used to measure the film thicknesses. A spectral range of 400–850 nm and an incident angle of 75° were used in these measurements. The instrument was controlled using a comprehensive software package (SpectraRay) for data acquisition, modeling, fitting, and reporting of ellipsometric data. The refractive index values were derived from ellipsometric parameters for hybrid thin films deposited on silicon substrates using the Cauchy model. The growth rate was calculated by dividing the measured thickness by the number of deposition cycles.

Fourier transform infrared spectroscopy (FTIR, Nicolet 4700) was performed over the wavenumber range of 650–4000 cm^{-1} using a glancing angle attenuated total reflectance (ATR, Harrick Scientific) sample holder with a Ge ATR crystal. The absorption spectra were typically averaged over 100 scans at a resolution of 2 cm^{-1}.

A cross-sectional transmission electron microscopy (TEM) sample was prepared by the lift-out method using a focused ion beam (FIB, FEI Nova 2000) equipped with a nano-manipulator. Prior to TEM sample preparation, zinc oxide (ZnO) was deposited using DEZ and water to protect the MALD films from ion beam damage. The sample was examined using a field emission TEM (JEOL 2100).

UV-Vis absorption spectra were measured in air using a spectrometer (Ocean Optics USB 4000) with a DT-mini-2-GS light source. The spectra were recorded using an uncoated glass substrate (PEARL) as a reference.

Thin film transistor (TFT) devices were fabricated for electrical characterization. Approximately 50 nm of HQ/DEZ was deposited for the channel layer, patterned using photolithography. Source and drain (S-D) metal contacts were patterned and deposited using lift-off approach. Following device fabrication, 10 nm of aluminum oxide (Al_2O_3) was deposited using trimethyl-aluminum (TMA) and water as ALD precursors at 100 °C to prevent decomposition of the channel material in air. A thermal post annealing process was performed at 200 °C for 1 hour in nitrogen (N_2).

Electrical measurement was performed using a Cascade probe station coupled to a Keithley 4200 measurement system. The temperature dependence of TFT performance was examined by heating the probe station chuck from room temperature (RT) to 150 °C in a nitrogen (N_2) atmosphere. All devices were characterized in the dark.

Hall-effect measurement (LakeShore, 8400 Series) was performed using Hall-bar configuration (see S.4) on MALD films deposited on a silicon substrate with approximately 300 nm of thermal oxide. Hall-bar devices with dimension of 1 mm in length and 135 μm in width were applied. The carrier type, carrier concentration, and Hall mobility were determined from Hall-effect measurements in a magnetic field of 1.24 T at room temperature.

Density functional theory (DFT) calculations were performed based on generalized gradient approximation (GGA) of Perdew-Burke-Ernzerhof method.[47] In order to accurately predict electronic excitation, the quasiparticle band energy is computed by single-shot G^0W^0 approach using Berkeley-GW code.[48, 49] The mean-field calculations are done with the Quantum-Espresso code, in which the plane wave cutoff energy is 40 Ry and all structures are fully relaxed as the residual atomic force is smaller than 0.001 eV from DFT. The k-point sampling of 1×1×24 is applied to 1-D system in DFT and GW calculations. In GW calculation, the cell wire truncation and cell box truncation methods are applied for 1-D molecule chain and single molecule, respectively to minimize the coulomb interaction among the periodic images. The generalized plasmon pole (GPP) approximation is used for frequency dependence of the dielectric matrix. The energy cutoff for the plane wave expansion of dielectric matrix is 6 Ry. Our photo spectrum calculation is based on GW plus Bethe–Salpeter equation (BSE) approach.[50]

Supporting Information

Experimental details for the confirmation of Ohmic contact between HQ/DEZ hybrid semiconductor and electrode, temperature dependence measurement of TFT devices, and device configuration of Hall-effect measurement.

AUTHOR INFORMATION

Corresponding Author

*E-mail: jiyoung.kim@utdallas.edu

ACKNOWLEDGMENTS

The authors would like to thank Prof. M. Quevedo-Lopez for using of his Hall-effect measurement equipment. All the calculations were performed using computational resources of Texas Advanced Computer Center (TACC) at University of Texas at Austin. This research is partially supported by Creative Materials Discovery Program through NRF (2015M3D1A1068061) and UTD-KMU InFUSION center through the Foreign Research Institute Program by MSIP, Korea, and SWAN center funded by NRI-SRC and NIST.

REFERENCES:

1. D. B. Mitzi, K. Chondroudis and C. R. Kagan, *IBM J. Res. Dev.*, 2001, **45**, 29-45.

2. C. R. Kagan, D. B. Mitzi and C. D. Dimitrakopoulos, *Science*, 1999, **286**, 945-947.

3. Y.-R. Lee, J. Kim and W.-S. Ahn, *Korean J. Chem. Eng.*, 2013, **30**, 1667-1680.

4. P. P. Boix, K. Nonomura, N. Mathews and S. G. Mhaisalkar, *Materials Today*, 2014, **17**, 16-23.

5. Q. Gao, P. Chen, Y. Zhang and Y. Tang, *Advanced Materials*, 2008, **20**, 1837-1842.

6. S. M. George, B. Yoon and A. A. Dameron, *Accounts of Chemical Research*, 2009, **42**, 498-508.

7. S. Cho, G. Han, K. Kim and M. M. Sung, *Angewandte Chemie International Edition*, 2011, **50**, 2742-2746.

8. H. Zhou and S. F. Bent, *ACS Applied Materials & Interfaces*, 2011, **3**, 505-511.

9. J. Kim and T. Kim, *JOM*, 2009, **61**, 17-22.

10. C. Bae, H. Yoo, S. Kim, K. Lee, J. Kim, M. M. Sung and H. Shin, *Chemistry of Materials*, 2008, **20**, 756-767.

11. P. Sivasubramani, T. J. Park, B. E. Coss, A. Lucero, J. Huang, B. Brennan, Y. Cao, D. Jena, H. Xing, R. M. Wallace and J. Kim, *physica status solidi (RRL) – Rapid Research Letters*, 2012, **6**, 22-24.

12. Y. J. Suh, N. Lu, S. Y. Park, T. H. Lee, S. H. Lee, D. K. Cha, M. G. Lee, J. Huang, S.-S. Kim, B.-H. Sohn, G.-H. Kim, M. J. Ko, J. Kim and M. J. Kim, *Micron*, 2013, **46**, 35-42.

13. J. Huang, M. Lee, A. Lucero, L. Cheng and J. Kim, *The Journal of Physical Chemistry C*, 2014, **118**, 23306-23312.

14. L. Cheng, X. Qin, A. T. Lucero, A. Azcatl, J. Huang, R. M. Wallace, K. Cho and J. Kim, *Acs Appl Mater Inter*, 2014, **6**, 11834-11838.

15. Q. Peng, B. Gong, R. M. VanGundy and G. N. Parsons, *Chemistry of Materials*, 2009, **21**, 820-830.

16. P. W. Loscutoff, H. Zhou, S. B. Clendenning and S. F. Bent, *ACS Nano*, 2010, **4**, 331-341.

17. A. I. Abdulagatov, R. A. Hall, J. L. Sutherland, B. H. Lee, A. S. Cavanagh and S. M. George, *Chemistry of Materials*, 2012, **24**, 2854-2863.

18. Y. Liang, J. Huang, P. Zang, J. Kim and W. Hu, *Applied Surface Science*, 2014, **322**, 202-208.

19. B. H. Lee, M. K. Ryu, S.-Y. Choi, K.-H. Lee, S. Im and M. M. Sung, *Journal of the American Chemical Society*, 2007, **129**, 16034-16041.

20. B. H. Lee, B. Yoon, V. R. Anderson and S. M. George, *The Journal of Physical Chemistry C*, 2012, **116**, 3250-3257.

21. P. Sundberg, A. Sood, X. Liu, L.-S. Johansson and M. Karppinen, *Dalton Transactions*, 2012, **41**, 10731-10739.

22. J. Huang, M. Lee, A. Lucero and J. Kim, *Chemical Vapor Deposition*, 2013, **19**, 142-148.

23. J. Huang, A. T. Lucero, L. Cheng, H. J. Hwang, M.-W. Ha and J. Kim, *Applied Physics Letters*, 2015, **106**, 123101.

24. J. W. Elam and S. M. George, *Chemistry of Materials*, 2003, **15**, 1020-1028.

25. K. B. Klepper, O. Nilsen and H. Fjellvag, *Dalton Transactions*, 2010, **39**, 11628-11635.

26. B. Gong, Q. Peng and G. N. Parsons, *The Journal of Physical Chemistry B*, 2011, **115**, 5930-5938.

27. A. A. Dameron, D. Seghete, B. B. Burton, S. D. Davidson, A. S. Cavanagh, J. A. Bertrand and S. M. George, *Chemistry of Materials*, 2008, **20**, 3315-3326.

28. P. Sundberg and M. Karppinen, *Beilstein Journal Nanotechnol.*, 2014, **5**, 1104-1136

29. B. Shong, K. T. Wong and S. F. Bent, *The Journal of Physical Chemistry C*, 2012, **116**, 4705-4713.

30. B. Yoon, Y. Lee, A. Derk, C. Musgrave and S. George, *ECS Transactions*, 2011, **33**, 191-195.

31. H. F. Clausen, Y.-S. Chen, D. Jayatilaka, J. Overgaard, G. A. Koutsantonis, M. A. Spackman and B. B. Iversen, *The Journal of Physical Chemistry A*, 2011, **115**, 12962-12972.

32. A. Sood, P. Sundberg and M. Karppinen, *Dalton Transactions*, 2013, **42**, 3869-3875.

33. J. I. J. I. Pankove, *Optical processes in semiconductors*, Prentice-Hall, 1971.

34. D. C. Olson, S. E. Shaheen, M. S. White, W. J. Mitchell, M. F. A. M. van Hest, R. T. Collins and D. S. Ginley, *Advanced Functional Materials*, 2007, **17**, 264-269.

35. Y.-J. Hwang, N. M. Murari and S. A. Jenekhe, *Polymer Chemistry*, 2013, **4**, 3187-3195.

36. B.-C. Shih, Y. Xue, P. Zhang, M. L. Cohen and S. G. Louie, *Physical Review Letters*, 2010, **105**, 146401.

37. D. Natali and M. Caironi, *Advanced Materials*, 2012, **24**, 1357-1387.

38. T.-J. Ha, P. Sonar and A. Dodabalapur, *Physical Chemistry Chemical Physics*, 2013, **15**, 9735-9741.

39. C. R. Newman, C. D. Frisbie, D. A. da Silva Filho, J.-L. Brédas, P. C. Ewbank and K. R. Mann, *Chemistry of Materials*, 2004, **16**, 4436-4451.

40. R. Rödel, F. Letzkus, T. Zaki, J. N. Burghartz, U. Kraft, U. Zschieschang, K. Kern and H. Klauk, *Applied Physics Letters*, 2013, **102**, 233303.

41. S.-H. K. Park, C.-S. Hwang, H.-S. Kwack, J.-H. Lee and H. Y. Chu, *Electrochemical and Solid-State Letters*, 2006, **9**, G299-G301.

42. N. Huby, S. Ferrari, E. Guziewicz, M. Godlewski and V. Osinniy, *Applied Physics Letters*, 2008, **92**, 023502.

43. Q. Wu, S. Ren, M. Wang, X. Qiao, H. Li, X. Gao, X. Yang and D. Zhu, *Advanced Functional Materials*, 2013, **23**, 2277-2284.

44. H. Usta, C. Risko, Z. Wang, H. Huang, M. K. Deliomeroglu, A. Zhukhovitskiy, A. Facchetti and T. J. Marks, *Journal of the American Chemical Society*, 2009, **131**, 5586-5608.

45. D. Liu, X. Xu, Y. Su, Z. He, J. Xu and Q. Miao, *Angewandte Chemie International Edition*, 2013, **52**, 6222-6227.

46. F. Zhang, C. Di, N. Berdunov, Y. Hu, Y. Hu, X. Gao, Q. Meng, H. Sirringhaus and D. Zhu, *Advanced Materials*, 2013, **25**, 1401-1407.

47. J. P. Perdew, K. Burke and M. Ernzerhof, *Physical Review Letters*, 1996, **77**, 3865-3868.

48. M. S. Hybertsen and S. G. Louie, *Physical Review B*, 1986, **34**, 5390-5413.

49. M. Rohlfing and S. G. Louie, *Physical Review B*, 2000, **62**, 4927-4944.

50. J. Deslippe, G. Samsonidze, D. A. Strubbe, M. Jain, M. L. Cohen and S. G. Louie, *Computer Physics Communications*, 2012, **183**, 1269-1289.